Faraday Discussions

Accepted Manuscript

This manuscript will be presented and discussed at a forthcoming Faraday Discussion meeting. All delegates can contribute to the discussion which will be included in the final volume.

Register now to attend! Full details of all upcoming meetings: http://rsc.li/fd-upcoming-meetings

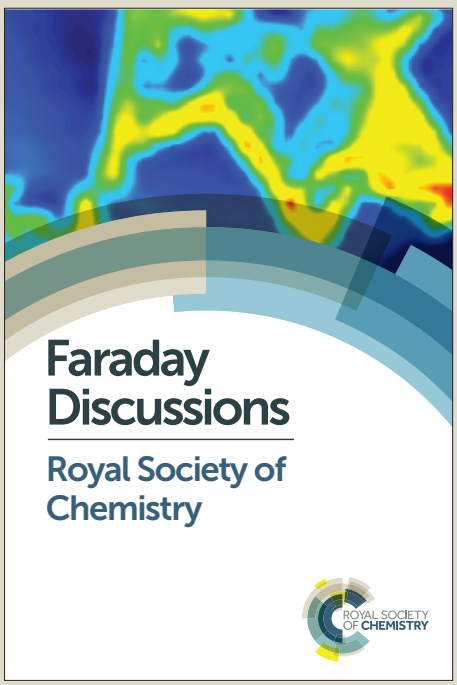

This is an *Accepted Manuscript*, which has been through the Royal Society of Chemistry peer review process and has been accepted for publication.

Accepted Manuscripts are published online shortly after acceptance, before technical editing, formatting and proof reading. Using this free service, authors can make their results available to the community, in citable form, before we publish the edited article. We will replace this *Accepted Manuscript* with the edited and formatted *Advance Article* as soon as it is available.

You can find more information about *Accepted Manuscripts* in the Information for Authors.

Please note that technical editing may introduce minor changes to the text and/or graphics, which may alter content. The journal's standard Terms & Conditions and the Ethical guidelines still apply. In no event shall the Royal Society of Chemistry be held responsible for any errors or omissions in this *Accepted Manuscript* or any consequences arising from the use of any information it contains.

ROYAL SOCIETY OF CHEMISTRY

www.rsc.org/faraday_d

Electrochemical stability of $Sm_{0.5}Sr_{0.5}CoO_{3-\delta}$-infiltrated YSZ for solid oxide fuel cells/electrolysis cells

Hui Fan, Minfang Han*
Department of Thermal Engineering, Tsinghua University, Beijing, 100084, China

*Corresponding author
E-mail: hanminfang@sina.com
Tel: +86 (010) 62790686
Fax: +86 (010) 62790686

Abstract: Composite SSC ($Sm_{0.5}Sr_{0.5}CoO_{3-\delta}$)-YSZ (yttria stabilized zirconia) oxygen electrodes were prepared by an infiltration process. X-ray diffraction (XRD) analysis and scanning electron microscopy (SEM) of the composite electrodes showed the formation of SSC perovskite and well-connected network of SSC particles in the porous YSZ backbone, respectively. Electrochemical performance of the cells was investigated under both fuel cell and steam electrolysis modes by using polarization curves and electrochemical impedance spectroscopy (EIS). The cell experienced a large degradation rate at 700 ^{o}C and a constant voltage of 0.7 V for over 100 h under power generation operation. The subsequent post-cell SEM micrograph revealed that agglomeration of the infiltrated SSC particles was possibly resulted into the performance deterioration. Further, a long-term stability of the cell was examined at 700 ^{o}C and a constant voltage of 1.3 V under steam electrolysis mode. SEM associated with energy dispersive X-ray spectroscopy (EDS) was employed to characterize the post-test cell after the long-term electrolysis operation. It indicated that besides the agglomeration of SSC particles, the delamination of the SSC-YSZ oxygen electrode from the YSZ electrolyte as well as segregation of cobalt-enrichment particles (particularly cobalt oxides) at the interface was probably responsible for the cell degradation under the steam electrolysis mode.

Keywords: Strontium-doped samarium cobaltite; Infiltration; Solid oxide fuel cell; Solid oxide electrolysis cell;

1. Introduction

A solid oxide fuel cell (SOFC) is an electrochemical device that can continuously convert chemical energy of a fuel directly into electrical energy [1]. SOFCs have the advantages of high efficiency and high fuels flexibility. At present, the most commonly used solid electrolyte in solid oxide fuel cells (SOFCs) is yttria-stabilized zirconia (YSZ) [2], which is a predominantly oxygen ion conductor with negligible electronic conductivity. Traditional Ni-based cermets anode has been extensively studied over the years to provide high performance for solid oxide fuel cells (SOFCs) [3, 4]. SOFCs served as an alternative in the near future show great promise for efficient and benign conversion of chemical energy into electricity. Solid oxide electrolysis cells (SOECs) inverse to SOFCs are the promising technologies to achieve zero-emission and high-purity hydrogen production [5]. Compared with low temperature operation, high temperature steam electrolysis in SOECs has reduced electrical energy demand and lower internal resistance of the

Faraday Discussions Accepted Manuscript

cell [6].

LSM (Sr-doped $LaMnO_3$) was widely used as oxygen electrode for the state-of-the-art SOFC/SOEC [7]. However, it is well known that LSM exhibits poor performance at reduced temperature for SOFC operation and suffers delamination from electrolyte for SOEC operation. Cobalt-containing perovskite oxides are under investigation for the oxygen electrode of SOFCs and have attracted much attention because of their mixed ionic/electronic conduction characteristics [8]. Strontium-doped cobaltites have been studied as cathode materials for SOFCs due to its high electrical conductivity and the low overpotential. Sr-doped $LaCoO_3$ (LSCo) has been infiltrated into porous YSZ backbone to prepare composite LSCo-YSZ electrode [9, 10]. The cell using the composite LSCo-YSZ electrode demonstrated high levels of performance and low cathode polarization. $Sm_{0.5}Sr_{0.5}CoO_{3-\delta}$ (SSC) perovskites have recently attracted attention as cathode materials for intermediate temperature SOFCs. In comparison with LSCo electrode, SSC electrode showed lower overpotential [8]. Nevertheless, it has been reported that the Sr-doped cobaltite perovskites undergo a solid state reaction with YSZ at the sintering temperature required for standard electrode preparation (usually over 1000 ^oC) [9, 11]. Nano-sized composite electrodes were fabricated by the infiltration technology and subsequently sintered at a relatively low temperature (700-900 ^oC) [12], which effectively hinder formation of the insulating phases. A study by Nicholas et al. [13] has shown that SSC nitrate solution was infiltrated into porous GDC scaffolds to prepare nano-composite SSC-GDC electrode, resulting into low cathode polarization resistance. Furthermore, influence from infiltrate solution concentration, infiltrate loading, and the number of infiltration steps on the cathode polarization was investigated. Zhang et al. [14] has reported that nano-sized SSC cathode was fabricated by an ion-impregnation process and embedded into porous SDC backbone for intermediate-temperature SOFCs with zirconia (ScSZ) electrolyte. The impregnated SSC-SDC composite electrode demonstrated extended triple phase boundary (TPB) length, reduced interfacial resistance, and improved power density. Except for the application of SOFC cathode, Sr-doped cobaltites can be employed into SOECs for hydrogen production from steam electrolysis. LSCo-YSZ composite was prepared and tested as SOEC anode to show comparable impedance with LSF (Sr-doped $LaFeO_3$ [15]. Further, composite SSC-SDC ($Sm_{0.2}Ce_{0.8}O_{1.9}$) oxygen electrodes have been investigated to exhibit lower polarization resistance than that of pure SSC electrode under steam electrolysis operating mode [16], which indicated that SSC composite was a promising oxygen electrode candidate for SOECs. Compared with standard LSCF-GDC cell, the SSC-infiltrated cells exhibited improved performance and significantly reduced electrode polarization resistance under both SOFC and SOEC modes.

Perovskite SSC composite has been demonstrated to show enhanced electrochemical property for both SOFC and SOEC operations. However, few investigations were focused on the electrochemical stability of the SSC-based oxygen electrode for both SOFCs and SOECs. In this study, nano-sized SSC-YSZ oxygen electrodes were prepared by an infiltration process for SOFCs/SOECs. The electrochemical performance of the cells was evaluated under both power generation and steam electrolysis modes. Long-term stability operation was carried out for both the oxygen reduction and oxidation reaction. Possible deterioration mechanisms of the cells under the two modes were proposed based on post-test scanning electron microscopy (SEM) analysis, associated with energy dispersive X-ray spectroscopy (EDS) characterization.

2. Experimental

2.1 Fabrication of porous cell substrates

Faraday Discussions Accepted Manuscript

As in our previous papers [17], the porous cell substrates have the configuration of Ni-YSZ hydrogen electrode/YSZ electrolyte/porous YSZ layer. Tape casting, hot isostatic pressing, and one-step sintering process were employed to fabricate the substrates. NiO-YSZ support was prepared by mixing nickel oxide powder, YSZ (TZ-8Y, Tosoh) and graphite (Furunda Zirconium Material Co. Ltd., China) pore former at a weight ratio of 50:50:10. Ethanol-butanone solvent, caster oil dispersant, dibutyl phthalate (DBP) plasticizer, and polyvinyl butyral (PVB) binder were then added and ball-milled to form NiO-YSZ slurry. The tape casting process for the NiO-YSZ support was obtained in our previous work [18]. The YSZ electrolyte was prepared by the same tape casing process as in the case of the NiO-YSZ substrates except for no addition of NiO powder and graphite powders. For the porous YSZ layer, 50 wt% graphite pore former was added to form backbone. The slurries for the NiO-YSZ support, YSZ electrolyte, and porous YSZ layer were separately cast via a tape casting machine (DR-150, made in Japan). These tapes were dried overnight in air atmosphere. One sheet of NiO-YSZ support (~300 μm), YSZ electrolyte layer (20~30 μm), and porous YSZ layer (~70 μm) were stacked together under a vacuum condition and laminated at 20 MPa for 10 min using a hot isostatic press (30Tm Shanxi, China) to form a NiO-YSZ supported tri-layer structure. The resulting tri-layer tape was punched to discs, and then co-sintered at 1300 ^{o}C for 10 h in order to densify the electrolyte layer, during which graphite was burned out, leaving a well-formed porous YSZ network. The microstructural characteristics of the fired tri-layer tapes were analyzed by using a scanning electron microscope, and the estimated porosity of the porous YSZ layer was 40~50%.

2.2 single-cell preparation

A precursor solution of SSC ($Sm_{0.5}Sr_{0.5}CoO_{3-\delta}$) for the infiltration was prepared by dissolving stoichiometric amounts of $Sm(NO_3)_3$•$6H_2O$, $Sr(NO_3)_2$ and $Co(NO_3)_2$•$6H_2O$ with chelating agent into de-ionized water [19]. Ethanol which has been proved to be an effective additive to lower surface tension of the infiltration solution was added into the aqueous solution [20]. The solution was then infiltrated into the pre-treated porous YSZ backbone by using a microsyringe. The infiltrated samples were dried at room temperature until the precursor solution fully permeated and then followed by firing at 450 ^{o}C for 1h to decompose the nitrate. The infiltration process was repeatedly carried out to achieve desired SSC loading amount. The infiltrated samples were eventually sintered at 850 ^{o}C for 5 h to prepare nano-structural NiO-YSZ/YSZ/SSC-YSZ cells.

2.3 Cell characterization and electrochemical measurement

The hydrogen electrode-supported single cell was mounted onto a horizontal alumina tube. Ceramic paste (Aramco-552, USA) was adopted as sealant. Silver paste (Ag ink, Beijing, China) was applied as a current collector onto electrode surfaces. Silver wires were pressed against the oxygen electrode to obtain sufficient electronic contact with both electrodes in four-wire set up. The cell was placed inside a temperature-controlled tube furnace and heated at a heating rate of 2 ^{o}C/min. when the temperature was increased to 700 ^{o}C, low flow rate of hydrogen gas was introduced for in-situ reduction of the NiO-YSZ hydrogen electrode. The area of electrolyte and hydrogen electrode was about 1.5 cm^2 and the geometrical area of oxygen electrode was 0.2 cm^2. For SOFC operation, humidified hydrogen gas (3% H_2O, volume fraction, the same below) with a flow rate of 50 sccm (standard cubic centimeters per minute) was fed to the Ni-based hydrogen electrode, whilst the oxygen electrode was exposed to an ambient atmosphere. For SOEC operation, 50% H_2O, 25% H_2 and 25% N_2 mixture gas at a total flow rate of 100 sccm was supplied to the hydrogen electrode. Similarly, the oxygen electrode was left open to the

Faraday Discussions Accepted Manuscript

atmospheric environment. During the SOEC testing, a thermostatic water bath was used at a constant temperature to maintain the desired steam content. Current density versus voltage curves (polarization curve) and electrochemical impedance spectra (EIS) under open circuit were measured at 650-800 ^{o}C by using electrochemical analyzers of Solartron 1287 and 1260, respectively. The EIS were recorded in the frequency range from 100 mHz to 100 kHz with AC amplitude of 20 mV. Additionally, a high power X-ray diffractometer (XRD, PANalytical X′ Pert PRO, Netherlands) loaded with CuKα radiation was employed to verify the crystallographic phase of the infiltrated SSC. Morphological and elemental characterizations of the pre- and post-test cells were carried out by using a scanning electron microscope (SEM, FEI Quanta 250 FEG) attached with an energy dispersive X-ray spectroscope (EDS). Long-term stability experiments (*I-t* curves) were potentiostatically conducted under both fuel cell and steam electrolysis modes.

3 Results and discussion

3.1 Phase structure of the composite SSC-YSZ electrode

$Sm_{0.5}Sr_{0.5}CoO_{3-\delta}$ (SSC) precursor solution was added into YSZ matrix and sequentially sintered at 850 ^{o}C to prepare the composite oxygen electrode. Fig. 1 shows the X-ray diffraction pattern of the SSC-infiltrated YSZ electrode. It illustrated that the perovskite phase SSC was formed into the as-sintered YSZ layer. It was reported that SSC was susceptible to react with YSZ at high temperatures (>900 ^{o}C) and there is a poor chemical compatibility between SSC and YSZ [21]. Here, no impurity phase is observable, which indicates that no chemical reaction occurs at this temperature between SSC and YSZ. In ref. [22], porous $Sm_{0.7}Sr_{0.3}CoO_{3-\delta}$ cathode was deposited on an YSZ electrolyte substrate by solution precursor plasma spraying. It demonstrated that single perovskite phase was formed when the deposits were annealed at 900 ^{o}C for 10 h. Zhang et al. [14] fabricated nano-structural SSC-SDC ($Sm_{0.2}Ce_{0.8}O_{1.9}$) electrode on zirconia (ScSZ, $Sc_{0.1}Zr_{0.89}Ce_{0.01}O_{2-x}$) electrolyte by an ion-impregnation process. No chemical reaction was presented between SSC and SDC at relatively low sintering temperature.

3.2 Microstructure characterization of the composite SSC-YSZ electrode

Fig. 2 illustrates the SEM cross-sectional morphologies of a freshly-prepared cell as well as its electrolyte and oxygen electrode. It can be seen from Fig. 2 (a) that dense YSZ electrolyte and porous oxygen electrode were formed after co-sintering at 1300 ^{o}C for 10 h. The YSZ electrolyte with a thickness of ~20 um maintains excellent adhesion with the SSC-YSZ oxygen electrode and no delamination/crack is presented at the electrolyte/oxygen electrode interface. We have reported that the porous YSZ layer prepared by the tape-casting and co-sintering process has a porosity of 40%~50% for the infiltration [18]. Fig. 2 (b) shows a higher magnification SEM image of the composite SSC-YSZ electrode prepared by the infiltration method. It can be observed that nano-sized SSC particles were uniformly covered onto the inner surface of the porous YSZ backbone. A well-connected network of SSC particles was formed through infiltration and in-situ calcination. The introduction of SSC particles provides the electron conductivity and increased active area of TPBs, which consequently improves the electrochemical performance of the composite oxygen electrode. Surface modification through the solution-based infiltration process has been demonstrated to be an effective approach for the enhancement of surface electrocatalytic activity and stability [23]. Wetting property of the precursor solution played a key role on the microstructure and morphology of the infiltrated catalyst coating. The addition of ethanol can dramatically improve the surface wetting property, resulting into the formation of uniform and continuous nano-catalyst particles [20].

Faraday Discussions Accepted Manuscript

3.3 Electrochemical performance of the cell under SOFC mode

The Ni-YSZ/YSZ/SSC-YSZ cells prepared by the infiltration process were initially evaluated under SOFC mode. For the SOFC operation, 3% H_2O humidified hydrogen gas at a flow rate of 50 sccm was introduced into the Ni-YSZ hydrogen electrode after the NiO was reduced into Ni. Voltage and power density vs current density curves of the cells in the operating temperature range of 650-800 ^oC were shown in Fig. 3 (a). The open circuit voltages (OCVs) of the cell are 1.047 V, 1.04 V, 1.035 V, and 1.03 V at the temperatures from 650 ^oC to 800 ^oC, respectively, which are slightly lower than the theoretical OCV values predicted from the Nernst Equation [24]. The all OCV values were over 1 V, indicating the YSZ electrolyte was dense and good sealing was achieved for the SOFC operation [25]. The dense electrolyte has also been demonstrated in SEM image of the cell in Fig. 2 (a). The cell shows maximum power densities of 776 $mW*cm^{-2}$, 530 $mW*cm^{-2}$, 327 $mW*cm^{-2}$, and 204 $mW*cm^{-2}$ from 800 ^oC to 650 ^oC, respectively. Huang et al. [26] have reported that composite LSF-YSZ cathode was formed by an impregnation process. The interfacial reaction can be effectively precluded at a low sintering temperature. Compared with conventional electrode fabrication such as screen printing, the composite electrode generally showed improved performance over SOFCs [27]. In this work, the cell exhibited relatively low performance, which may be ascribable to low SSC loading mount (~30 wt%). Fig. 3 (b) demonstrated the EIS plots of the cell under OCV condition at different temperatures. The EIS is composed of both ohmic and polarization resistances. The ohmic resistance (R_Ω) is usually obtained from high-frequency intercept with the real axis, representing the sum of the electrolyte resistance of ionic transfer, lead resistance of electronic transfer, and electrode/electrolyte contact resistance [28]. During the measurement, silver wires were used as current collectors to minimize the contribution of the lead resistance. The polarization resistance (R_p), calculated from the difference between high-frequency and low-frequency intercepts with the real axis, corresponds to catalytic oxygen reduction/oxidation, gas diffusion, ionic transport, and ion transfer between the electrodes and electrolyte [29]. In Nyquist plots, two distinct depressed arcs as high-frequency resistance and low-frequency resistance were displayed, indicating at least two different electrode processes. The high-frequency resistance with high temperature dependence is possibly associated with charge transfer process, while the low temperature dependence of low-frequency arc may be ascribed to diffusion processes composed of the adsorption-desorption of oxygen, oxygen diffusion at the gas-oxygen electrode interface, and the surface diffusion of the intermediate oxygen species [30]. It can be found from Fig. 3 (b) that the ohmic resistances of the cell were 0.13 $\Omega\ cm^2$, 0.18 $\Omega\ cm^2$, 0.25 $\Omega\ cm^2$, and 0.36 $\Omega\ cm^2$ at the temperatures from 800 ^oC to 650 ^oC, respectively. These ohmic resistances were much larger than those reported by other studies [31, 32] and may not be from electrolyte contribution alone. Additionally, interfacial resistance, electrode resistance, and contact resistance were also important contributions. The corresponding R_p values of 0.35 $\Omega\ cm^2$, 0.48 $\Omega\ cm^2$, 0.78 $\Omega\ cm^2$, and 1.77 $\Omega\ cm^2$ at 800 ^oC, 750 ^oC, 700 ^oC, and 650 ^oC, respectively were displayed in the EIS plots. A study by Lu et al. [33] has investigated that $Sm_{0.6}Sr_{0.4}CoO_{3-\delta}$ perovskite nanoparticles were incorporated into LSM-YSZ cathode by an infiltration process. With the infiltrated SSC nanoparticles into the cathode, the R_p of the cell was largely diminished. Furthermore, active-conductive $Ce_{0.8}Sm_{0.2}O_{1.9}$ (SDC) nanoparticles were infiltrated into a porous SSC electrode [34]. Compared to electrode performance for the electrode fabricated by screen printing, the catalytic activity towards oxygen dissociation of SSC prepared by the infiltration process was enhanced. In addition, LSCF ($La_{0.8}Sr_{0.2}Co_{0.5}Fe_{0.5}O_{3-\delta}$) cathode was

Faraday Discussions Accepted Manuscript

impregnated with nano-sized Pd and GDC particles [35]. The nano-structural Pd-LSCF and GDC-LSCF composite electrodes demonstrated lower polarization resistance and higher electrocatalytic activities than the pure LSCF electrode.

3.4 Long-term durability of the cell under SOFC mode and corresponding microstructure of the post-test cell

An electrochemical stability of the Ni-YSZ/YSZ/SSC-YSZ cell was investigated under potentiostatic test conditions. Fig. 4 displays the long-term durability of the cell operated at 700 ^{o}C and 0.7 V under fuel cell mode with humidified H_2 as fuel gas for over 100 h. The cell with SSC-infiltrated YSZ oxygen electrode suffered a rapid and continuous degradation in the time range of 50 h and then experienced a relatively stable current during this period from 50 h to 100 h. An operational stability of LSF-infiltrated YSZ electrodes has been examined by Wang et al. [31]. They reported an appreciably increase of the electrode polarization loss for a period of more than 2500 h. Similarly, SSC-infiltrated YSZ cells also have been investigated in ref. [36] for evaluating its operational stability under SOFC mode. An electrode polarization resistance vs time curve demonstrated that the SSC-YSZ composite electrode was gradually deteriorated with the increased polarization resistance. Microstructural changes play a vital role in the performance deterioration for the nano-sized electrode [37]. An SEM micrograph of the post-test SSC-infiltrated YSZ electrode under long-term power generation condition was shown in Fig. 5. Compared with the microstructure of the freshly prepared SSC-YSZ in Fig. 2 (b), the infiltrated SSC particles in the post-test cell were agglomerated and further partly separated from the YSZ scaffold. The performance degradation is likely associated with the growth and reduced interconnectivity of the nano-sized SSC particles [38]. Further, the particle coarsening would lead to a decrease in the electrochemical reaction sites, *i. e.* the TPB, and a increase in charge transfer resistance [37]. In addition, the particle agglomeration also decreases the porosity of the infiltrated electrode and affects the mass transfer rate of the oxygen reduction reaction. These results revealed that the agglomeration of the infiltrated SSC nanoparticles was possibly responsible for the degradation of the cell long-term performance.

3.5 Electrochemical performance of the cell under SOEC mode

The electrochemical reactions that take place in an SOEC are the inverse ones to those that take place in a solid oxide fuel cell (SOFC). Fig. 6 shows electrochemical performance of the Ni-YSZ/YSZ/SSC-YSZ cells under steam electrolysis mode. For the SOEC operation, steam containing a mixture of 50% H_2O, 25% H_2 and 25% N_2 was supplied to the Ni-YSZ hydrogen electrode side, acting as a reactant and the oxygen electrode was exposed to air atmosphere. Hydrogen was then produced at the hydrogen electrode side, whilst oxygen ions were transported to the oxygen electrode through the dense YSZ electrolyte under the action of electrolysis current, and thus oxygen gas was produced at the SSC-YSZ oxygen electrode [39]. The current-voltage characteristics of the cell at the temperatures of 800-650 ^{o}C were evaluated in Fig. 6 (a). The measured OCVs in the steam electrolysis condition were 0.91 V, 0.93 V, 0.95 V, and 0.96 V in the temperature range of 800 ^{o}C to 650 ^{o}C, respectively. According to the Nernst equation, steam/hydrogen gas ratio and temperature affect the OCV values [40]. The open circuit voltage of the cell clearly decreases with enlarging the temperature as be expected. It can be noted that the current densities of the cell at the electrolysis voltage of 1.3 V were 0.91 mA*cm^{-2}, 0.70 mA*cm^{-2}, 0.45 mA*cm^{-2}, and 0.27 mA*cm^{-2} at 800 ^{o}C, 750 ^{o}C, 700 ^{o}C, and 650 ^{o}C, respectively. It indicated higher current density was achieved with increasing the temperature at a given electrolysis voltage,

Faraday Discussions Accepted Manuscript

contributing to improved hydrogen production [41]. Furthermore, increased operation temperature can reduce electrolyte electrical resistance and improve electrode surface activity and electrolysis efficiency [42]. Typical Nyquist EIS at open circuits for the cells under the steam electrolysis mode are shown in Fig. 6 (b). It can be found that the R_Ω values of 0.27 Ω cm^2, 0.28 Ω cm^2, 0.30 Ω cm^2, and 0.40 cm^2 at the 800 ^oC to 650 ^oC, respectively, were similar to those obtained from fuel cell operation. The overall cell resistances were 0.50 Ω cm^2, 0.58 Ω cm^2, 0.96 Ω cm^2, and 1.64 Ω cm^2 in the temperature range from 800 ^oC to 650 ^oC, respectively. The total cell resistances were rapidly increased with decreasing the temperature, which was mainly due to the significant increase in the electrode polarization. The Rp values largely altered from 0.23 Ω cm^2 at 800 ^oC to 1.25 Ω cm^2 at 650 ^oC. It can be seen that the impedance spectra in Fig. 6 (b) were nearly unchanged to those in Fig. 3 (b). In agreement with other studies [43, 44], the cell revealed no real change in electrode performance as it operated from anodic to cathodic behavior.

3.6 Long-term durability of the cell under SOEC mode and subsequent microstructure of the post-test cell attached with EDS characterization

A long-term stability of the Ni-YSZ/YSZ/SSC-YSZ cell was potentiostatically tested under steam electrolysis mode. Fig. 7 depicts the long-term durability of the cell at 700 ^oC and an electrolysis voltage of 1.3 V for more than 100 h. For the long-term durability operation under SOEC mode, a mixture gas of 50% H_2O, 25% H_2 and 25% N_2 was introduced to the hydrogen electrode as reactant gas while the oxygen electrode was left to the atmospheric environment. It can be seen that the cell under electrolysis condition experienced a gradient degradation during the test period of over 100 h. The long-term durability of SOECs has been widely studied [45]. It has been reported that an overall voltage degradation rate of 3.8% kh^{-1} was achieved for a Ni-YSZ/YSZ/GDC/LSCF cell under SOEC operation [32]. It was found that SOEC degradation normally depends on the testing conditions, such as current density, steam content in fuel gas, temperature, etc. Moreover, LSM-YSZ composite has been investigated as the oxygen electrode for the steam electrolysis for 200 h. Rapid deterioration was revealed in 50 h [6]. The cell performance degradation was likely associated with its microstructural variation [46]. An SEM micrograph as well as the selected area EDS spectrum of the cell after the long-term steam electrolysis operation was shown in Fig. 8. As indicated by Fig. 8 (a), a gap was clearly formed between the SSC-YSZ oxygen electrode and the YSZ electrolyte, indicating the delamination of the oxygen electrode and thus the cell failure. The oxygen electrode delamination leading to the cell deterioration under the SOEC mode has been reported [6, 46-48]. Chen et al. [46] reported that the delamination of LSM oxygen electrode from YSZ electrolyte was due to the local tensile strains within the LSM particles and subsequent formation of microcracks and nanoparticles at the oxygen electrode/electrolyte interface. Additionally, high oxygen evolution rate into any defects at the perovskite-zirconia interfaces could lead to localized pressure-induced cracking at the interface [11]. Furthermore, the agglomeration of the SSC particles occurred under the steam electrolysis condition, just as that in the fuel cell mode. Both the delamination of the oxygen electrode from electrolyte and the agglomeration of SSC particles contributed to the cell degradation under steam electrode mode. An EDS spectrum of the selected area in the SEM image was exhibited in Fig. 8 (b). It was suggested that high content of cobalt was presented at the oxygen electrode/electrolyte interface. Ref. [46] also revealed the disintegration of the LSM particles at the oxygen electrode/electrolyte interface to form nanoparticles. The formation of lanthanum zirconate has been determined at the interface of YSZ electrolyte and LSM oxygen

Faraday Discussions Accepted Manuscript

electrode under anode polarization by Keane et al. [48]. By applying a large cathode polarization to SOFC, manganese oxides can be precipitated from the LSM electrode material [49]. Additionally, Co-rich particles was reported to be segregated on LSCF electrode surface in the EDS spectrum [50]. Thus, according to the EDS spectrum it was likely that cobalt-enrichment particles (particularly cobalt oxides) were segregated from the infiltrated SSC composite at the electrolyte/oxygen electrode interface under the electrolysis, which requires further experimental verification.

4. Conclusion

An SSC-YSZ oxygen electrode was prepared by the infiltration process for both SOFCs and SOECs with NiO-YSZ as hydrogen electrode and YSZ as electrolyte. The electrochemical performance as well as the long-term stability was investigated under power generation and steam electrolysis modes by using polarization curves and electrochemical impedance spectroscopy. SEM attached with EDS was employed to examine the microstructure changes of the cells before and after long-term stability under the both modes. Agglomeration of the infiltrated SSC particles was resulted into the cell performance degradation under long-term power generation mode. Whereas, besides the agglomeration of SSC particles, delamination of the SSC-YSZ oxygen electrode from the YSZ electrolyte along with deposition of cobalt-rich particles (most likely cobalt oxides) at the interface was possibly responsible for the cell deterioration after long-term steam electrolysis.

Acknowledgements

This work was supported by the National Basic Research Program of China (Grant No. 2012CB215404).

References

1 M. C. Williams, J. P. Strakey, W. A. Surdoval and L. C. Wilson, *Solid State Ionics*, 2006, **177**, 2039-2044.
2 P. Ried, C. Lorenz, A. Brönstrup, T. Graule, N. H. Menzler, W. Sitte and P. Holtappels, *J. Eur. Ceram. Soc.,* 2008, **28**, 1801-1808.
3 W. Z. Zhu and S. C. Deevi, *Mater. Sci. Eng. A*, 2003, **362**, 228-239.
4 M. Pihlatie, A. Kaiser and M. Mogensen, *J. Eur. Ceram. Soc.*, 2009, **29**, 1657-1664.
5 X. Wang, B. Yu, W. Q. Zhang, J. Chen, X. Luo and K. Stephan, *Int. J. Hydrogen Energy*, 2012, **37**, 12833-12838.
6 P. Kim-Lohsoontorn, Y.-M. Kim, N. Laosiripojana and J. Bae, *Int. J. Hydrogen Energy,* 2011, **36,** 9420-9427.
7 J. C. Ruiz-Morales, D. Marrero-López, J. Canales-Vázquez and J. T. S. Irvine, *RSC Advances*, 2011, **1**, 1403-1414.
8 H. Fukunaga, M. Koyama, N. Takahashi, C. Wen and K. Yamada, *Solid State Ionics*, 2000, **132**, 279-285.
9 Y. Huang, K. Ahn, J. M. Vohs and R. J. Gorte, *J. Electrochem. Soc.*, 2004, **151**, A1592-1597.
10 R. Küngas, F. Bidrawn, J. M. Vohs and R. J. Gorte, *J. Electrochem. Soc.,* 2010, **13**, B87-B90.
11 J. R. Mawdsley, J. D. Carter, A. J. Kropf, B. Yildiz and V. A. Maroni, *Int. J. Hydrogen Energy*, 2009, **34**, 4198-4207.
12 J. M. Vohs and R. J. Gorte, *Adv. Mater.*, 2009, **21**, 943-956.
13 J. D. Nicholas and S. A. Barnett, *J. Electrochem. Soc.*, 2010, **157**, B536-541.
14 H. Zhang, F. Zhao, F. L. Chen and C. R. Xia, *Solid State Ionics*, 2011, **192**, 591-594.
15 W. Wang, Y. Huang, S. Jung, J. M. Vohs and R. J. Gorte, *J. Electrochem. Soc.*, 2006, **153**, A2066-A2070.
16 W. Jiang, Z. Lü, B. Wei, Z. H. Wang, X. B. Zhu, Y. T. Tian, X. Q. Huang and W. H. Su, *Fuel Cells*, 2014, **14**, 76-82.
17 H. Fan, M. Keane, N. Li, D. Tang, P. Singh and M. F. Han, *Int. J. Hydrogen Energy*, 2014, **39**,

Faraday Discussions Accepted Manuscript

14071-14078.
18 Z. Liu, Z.-W. Zheng, M.-F. Han and M.-L. Liu, *J. Power Sources*, 2010, **195**, 7230-7233.
19 K. F. Chen, N. Ai and S. P. Jiang, *Electrochem. Commun.*, 2012, **19**, 119-122.
20 X. Y. Lou, Z. Liu, S. Z. Wang, Y. H. Xiu, C. P. Wong and M. L. Liu, *J. Power Sources,* 2010, **195**, 419-424.
21 H.Y. Tu, Y. Takeda, N. Imanishi and O. Yamamoto, *Solid State Ionics*, 1997, **100,** 283-288.
22 C.-X. Li, S. Liu, Y. Zhang and C.-J. Li, *Int. J. Hydrogen Energy*, 2012, **37**, 13097-13102.
23 D. Ding, X. X. Li, S. Y. Lai, K. Gerdes and M. L. Liu, Energy Environ. Sci., 2014, **7**, 552-575.
24 M. A. Laguna-Bercero, J. A. Kilner and S.J. Skinner, *Solid State Ionics*, 2011, **192**, 501-504.
25 M. F. Liu, J. F. Gao, X. Q. Liu and G. Y. Meng, *Int. J. Hydrogen Energy*, 2011, **36**, 13741-13745.
26 Y. Huang, J. M. Vohs and R. J. Gorte, *J. Electrochem. Soc.*, 2004, **151**, A646-651.
27 J. Chen, F. L. Liang, L. Liu, S. P. Jiang, B. Chi, J. Pu and J. Li, *J. Power Sources*, 2008, **183**, 586-589.
28 Y.-C. Chang, M.-C. Lee, W.-X. Kao, C.-H. Wang, T.-N. Lin and J.-C. Chang, *J. Taiwan Inst. Chem. Eng.* 2011, **42**, 775-782.
29 T. Ishihara, M. Honda, T. Shibayama, H. Minami, H. Nishguchi and Y. Takita, *J. Electrochem. Soc.,* 1998, **145**, 3177-3183.
30 W. Zhou, Z. P. Shao, F. L. Liang, Z.-G. Chen, Z. H. Zhu, W. Q. Jin and N. P. Xu, *J. Mater. Chem.*, 2011, **21**, 15343-15351.
31 W. Wang, M. D. Gross, J. M. Vohs and R. J. Gorte, *J. Electrochem. Soc.,* 2007, **154**, B439-445.
32 F. Tietz, D. Sebold, A. Brisse and J. Schefold, *J. Power Sources*, 2013, **223**, 129-135.
33 J. M. Serra, V. B. Vert, O. Büchler, W. A. Meulenberg and H. P. Buchkremer, *Chem. Mater.*, 2008, **20**, 3867-3875.
34 T. Z. Wu, Y. Q. Zhao, R. R. Peng and C. R. Xia, *Electrochim. Acta*, 2009, **54**, 4888-4892.
35 J. Chen, F. L. Liang, B. Chi, J. Pu, S. P. Jiang and L. Jian, *J. Power Sources*, 2009, **194**, 275-280.
36 F. C. Wang, D. J. Chen and Z. P. Shao, *J. Power Sources,* 2012, **216**, 208-215.
37 Y. H. Liu, F. Z. Wang, B. Chi, J. Pu, L. Jian and S. P. Jiang, *J. Alloys Compd.*, 2013, **578**, 37-43.
38 S. Lee, N. Miller, and K. Gerdes, *J. Electrochem. Soc.*, 2012, **159**, F301-F308.
39 B. Zhu, I. Albinsson, C. Andersson, K. Borsand, M. Nilsson and B.-E. Mellander, *Electrochem. Commun.,* 2006, **8**, 495-498.
40 B. Annabelle, J. Schefold, M. Zahid, *Int. J. Hydrogen Energy*, 2008, **33**, 5375-5382.
41 C. H. Yang, C. Jin, A. Coffin and F. L. Chen, *Int. J. Hydrogen Energy*, 2010, **35**, 5187-5193.
42 S. K. Mazloomi and N. Sulaiman, *Renewable Sustainable Energy Rev.*, 2012, **16**, 4257-4263.
43 J. E. O'Brien, *J. Heat Transfer*, 2012, **134**, 031017-01.
44 M. A. Laguna-Bercero, N. Kinadjan, R. Sayers, H. El Shinawi, C. Greaves and S. J. Skinner, *Fuel Cells*, 2011, **11**, 102-107.
45 S. D. Ebbesen, S. H. Jensen, A. Hauch and M. B. Mongensen, *Chem. Rev.*, 2014, **114**, 10697-10734.
46 K. F. Chen and S. P. Jiang, *Int. J. Hydrogen Energy*, 2011, **36**,10541-10549.
47 A. V. Virkar, *Int. J. Hydrogen Energy*, 2010, **235**, 9527-9543.
48 M. Keane, M. K. Mahapatra, A. Verma and P. Singh, *Int. J. Hydrogen Energy*, 2012, **37**, 16776-16785.
49 E. Park, S. Taniguchi, T. Daio, J.-T. Chou and K. Sasaki, *Int. J. Hydrogen Energy*, 2014, **19**, 1463-1475.
50 L. Zhao, J. Drennan, C. Kong, S. Amarasinghe and S. P. Jiang, *ECS Trans.*, 2013, **57**, 599-604.

Faraday Discussions Accepted Manuscript

Faraday Discussions Accepted Manuscript

Figure captions

Fig. 1 XRD diffraction pattern of an SSC-infiltrated YSZ oxygen electrode after firing at 850 ^{o}C.

Fig. 2 Typical SEM micrographs of (a) the cross section of the YSZ electrolyte and SSC-YSZ electrode and (b) a higher magnification image of the SSC-infiltrated composite electrode.

Fig. 3 (a) Voltage and power density vs current density curves, and (b) Nyquist electrochemical impedance spectra (EIS) under open circuit conditions at 650-800 ^{o}C for Ni-YSZ/YSZ/SSC-YSZ cell under SOFC mode

Fig. 4 Long-term durability operation of the Ni-YSZ/YSZ/SSC-YSZ cell at 700 ^{o}C and a constant voltage of 0.7 V under the fuel cell mode

Fig. 5 SEM micrograph of post-test SSC-YSZ composite electrodes under long-term power generation mode

Fig. 6 (a) Voltage and current density curves, and (b) Nyquist EIS under OCV at 658-800 ^{o}C for the Ni-YSZ/YSZ/SSC-YSZ cell with 50% H_2O, 25% H_2 and 25% N_2 fed to the hydrogen electrode under SOEC mode

Fig. 7 Long-term durability operation of the Ni-YSZ/YSZ/SSC-YSZ cell at 700 ^{o}C and a constant voltage of 1.3 V under the steam electrolysis mode

Fig. 8 (a) SEM micrograph of post-test cell under long-term steam electrolysis mode, and (b) EDS spectrum of the selected area in the SEM image

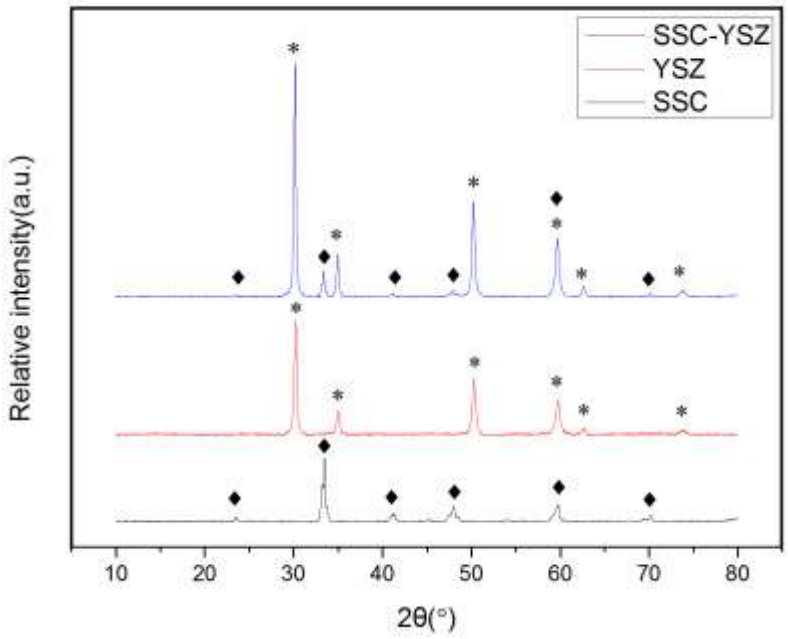

Fig. 1 XRD diffraction pattern of an SSC-infiltrated YSZ oxygen electrode after firing at 850 oC.
287x201mm (150 x 150 DPI)

Faraday Discussions Accepted Manuscript

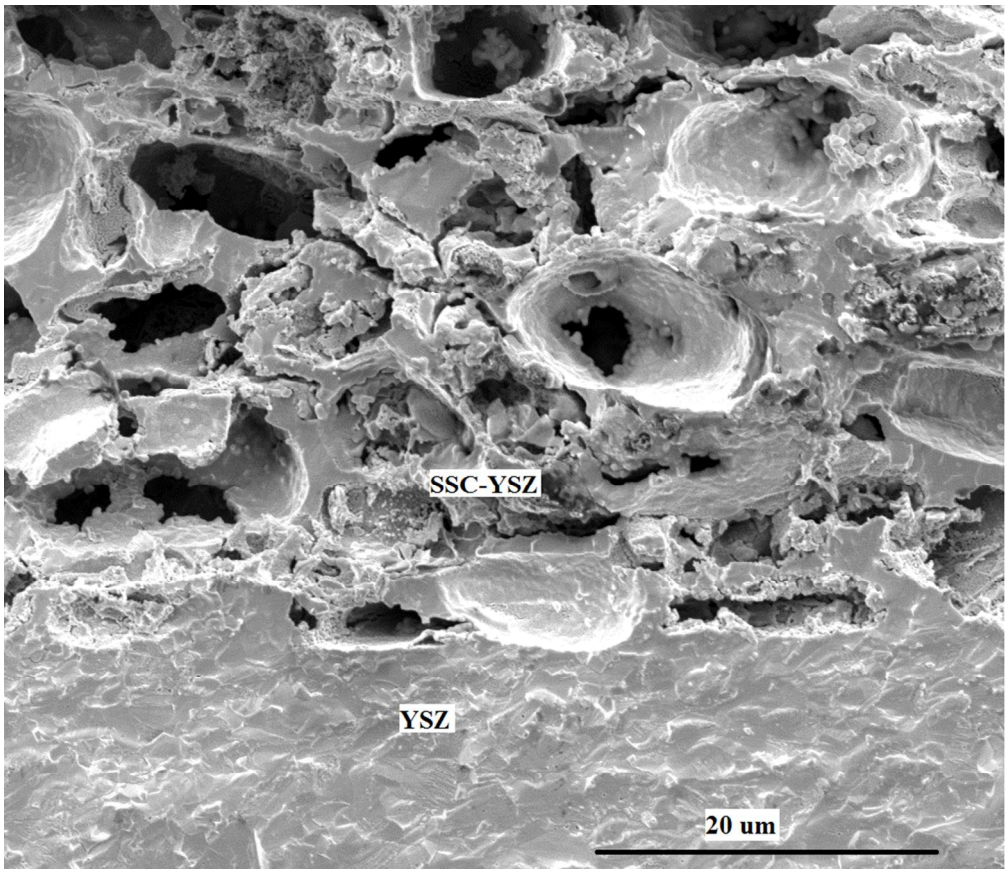

Fig. 2 Typical SEM micrographs of (a) the cross section of the YSZ electrolyte and SSC-YSZ electrode
302x260mm (86 x 86 DPI)

Faraday Discussions Accepted Manuscript

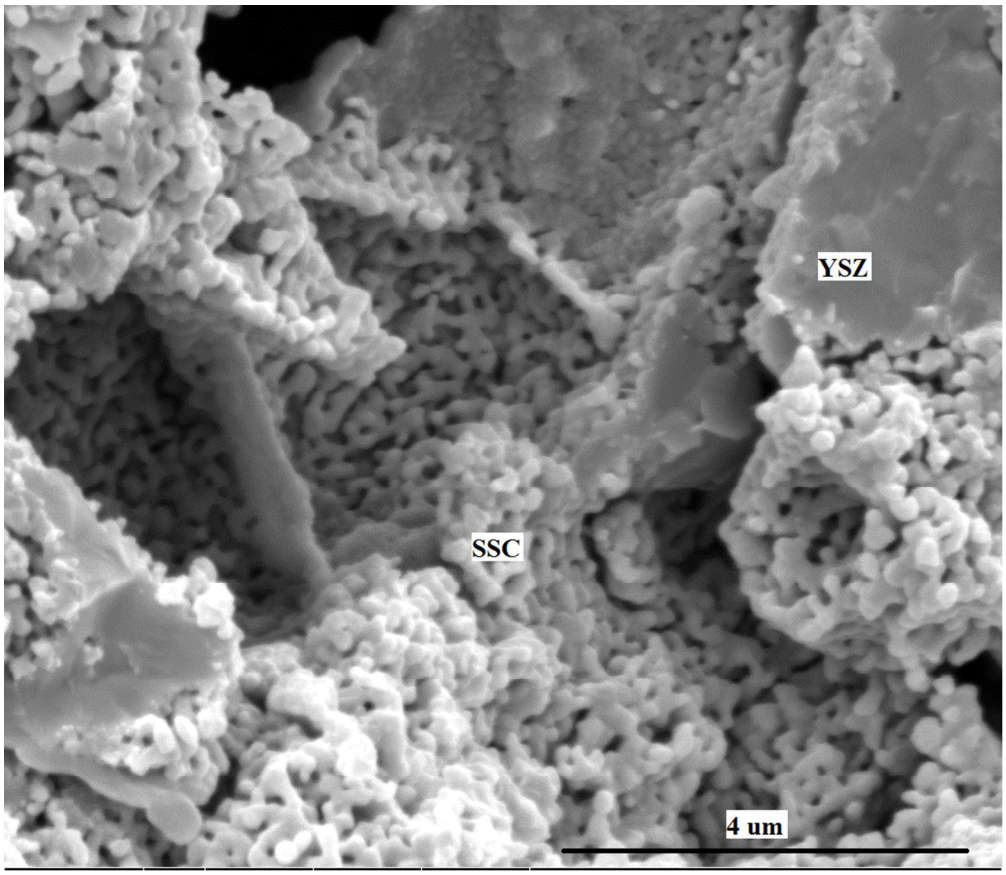

Figure 2(b) a higher magnification image of the SSC-infiltrated composite electrode
302x261mm (86 x 86 DPI)

Faraday Discussions Accepted Manuscript

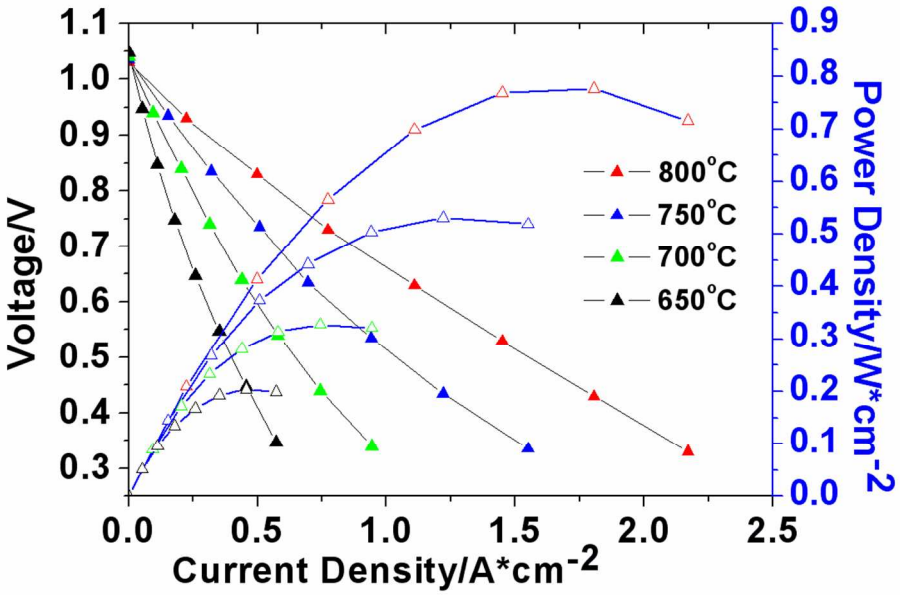

Fig. 3 (a) Voltage and power density vs current density curves at 650-800 oC for Ni-YSZ/YSZ/SSC-YSZ cell under SOFC mode
305x211mm (100 x 100 DPI)

Faraday Discussions Accepted Manuscript

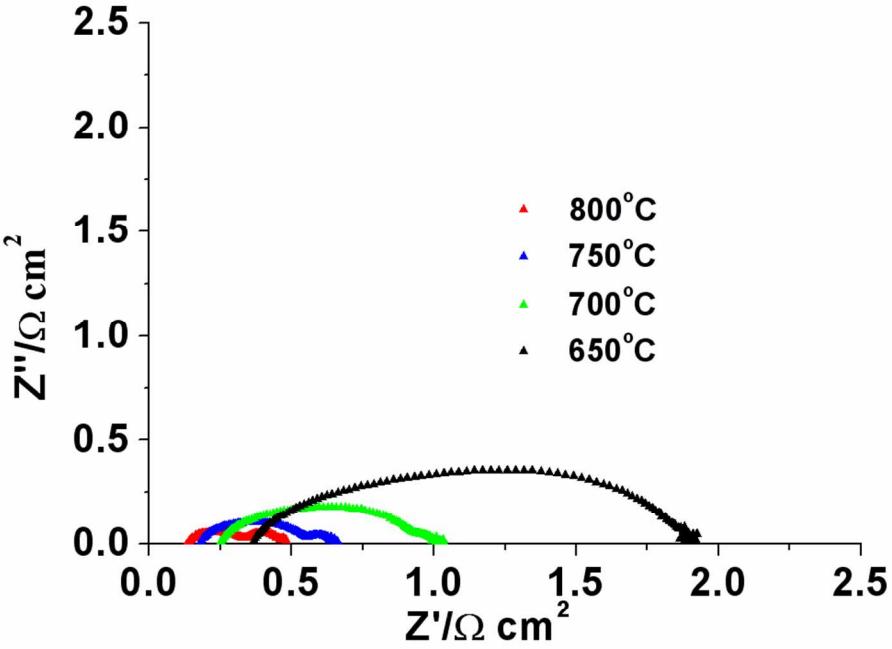

Figure 3(b) Nyquist electrochemical impedance spectra (EIS) under open circuit conditions at 650-800 oC for Ni-YSZ/YSZ/SSC-YSZ cell under SOFC mode
276x211mm (100 x 100 DPI)

Faraday Discussions Accepted Manuscript

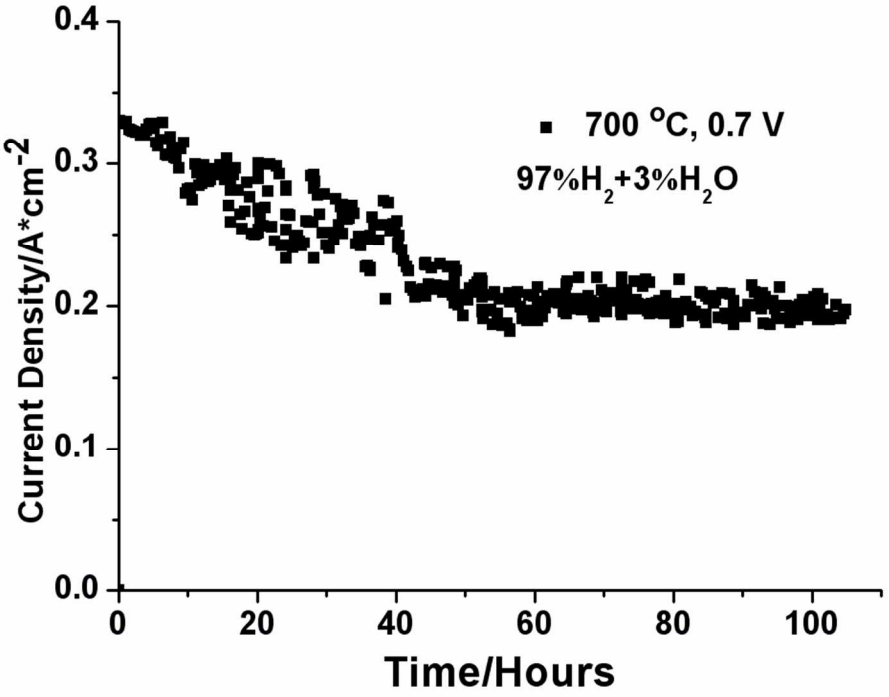

Fig. 4 Long-term durability operation of the Ni-YSZ/YSZ/SSC-YSZ cell at 700 oC and a constant voltage of 0.7 V under the fuel cell mode
265x215mm (100 x 100 DPI)

Faraday Discussions Accepted Manuscript

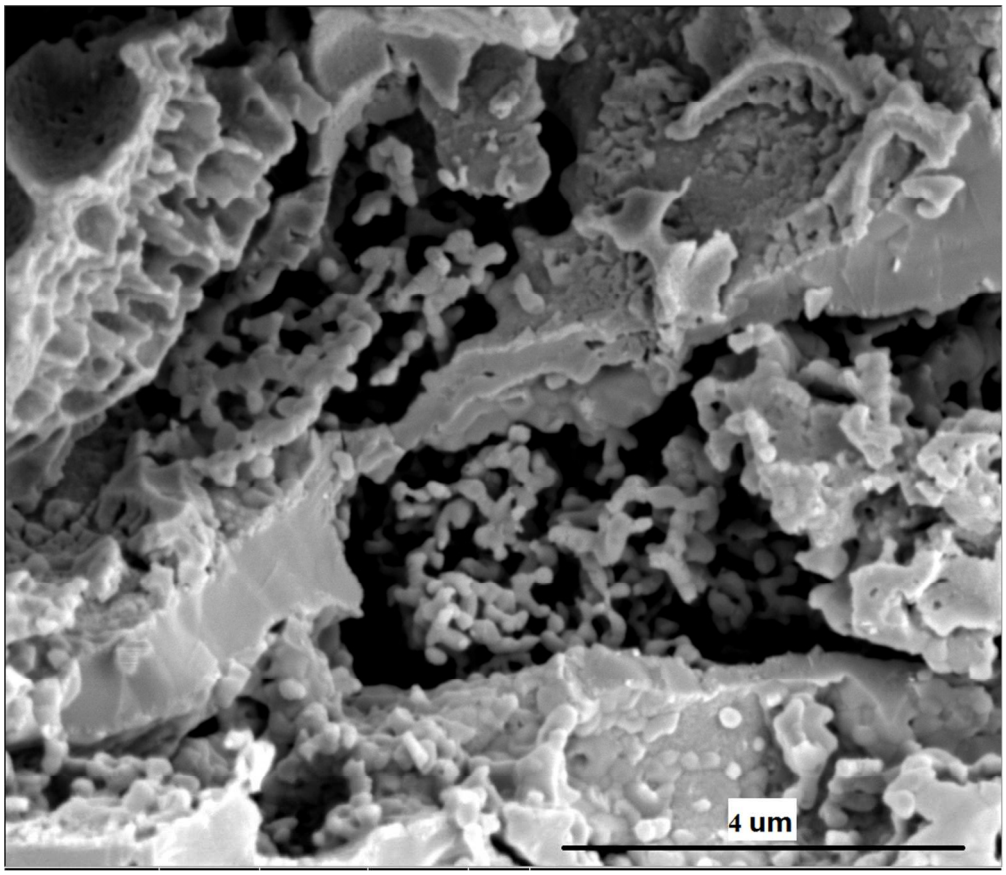

Fig. 5 SEM micrograph of post-test SSC-YSZ composite electrodes under long-term power generation mode
302x261mm (86 x 86 DPI)

Faraday Discussions Accepted Manuscript

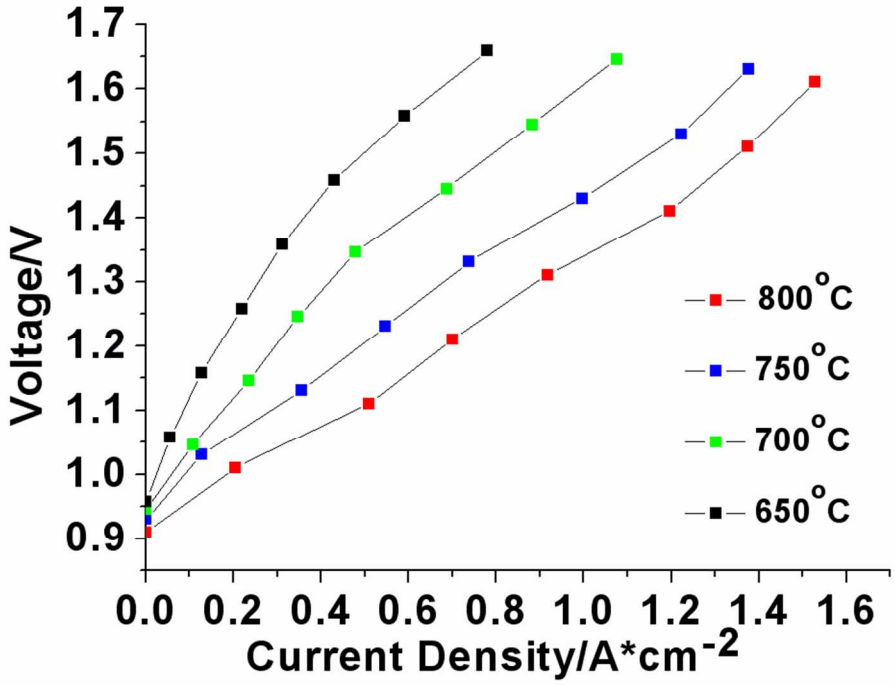

Fig. 6 (a) Voltage and current density curves at 658-800 oC for the Ni-YSZ/YSZ/SSC-YSZ cell with 50% H2O, 25% H2 and 25% N2 fed to the hydrogen electrode under SOEC mode
264x211mm (100 x 100 DPI)

Faraday Discussions Accepted Manuscript

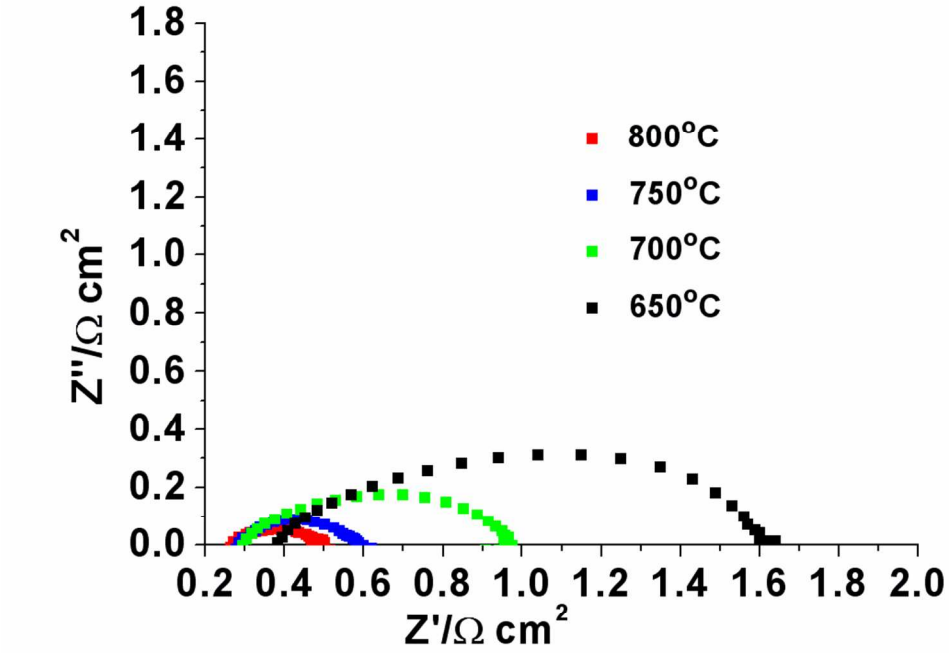

Figure 6 (b) Nyquist EIS under OCV at 658-800 oC for the Ni-YSZ/YSZ/SSC-YSZ cell with 50% H2O, 25% H2 and 25% N2 fed to the hydrogen electrode under SOEC mode
276x212mm (100 x 100 DPI)

Faraday Discussions Accepted Manuscript

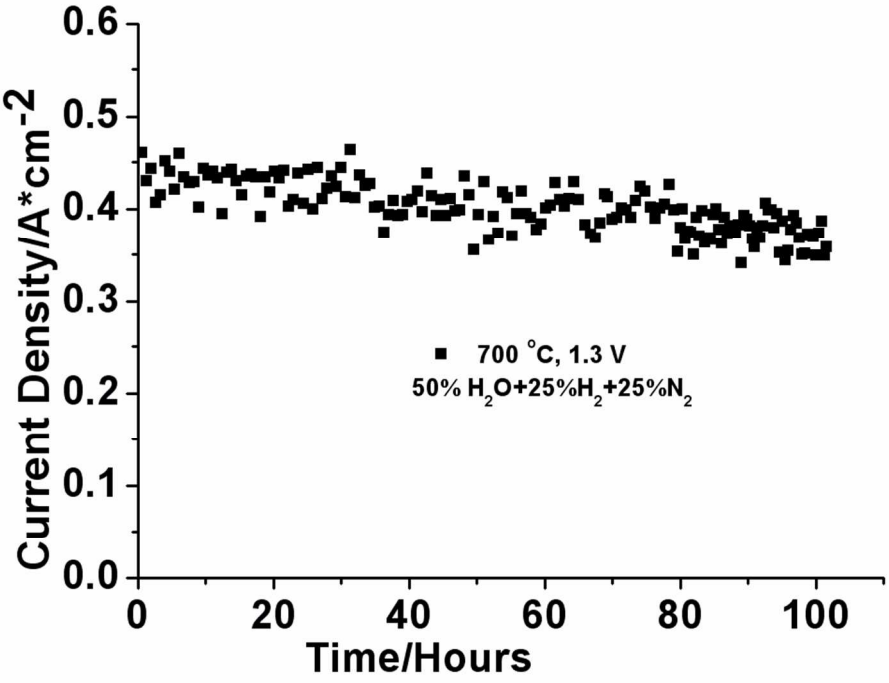

Fig. 7 Long-term durability operation of the Ni-YSZ/YSZ/SSC-YSZ cell at 700 oC and a constant voltage of 1.3 V under the steam electrolysis mode
272x217mm (100 x 100 DPI)

Faraday Discussions Accepted Manuscript

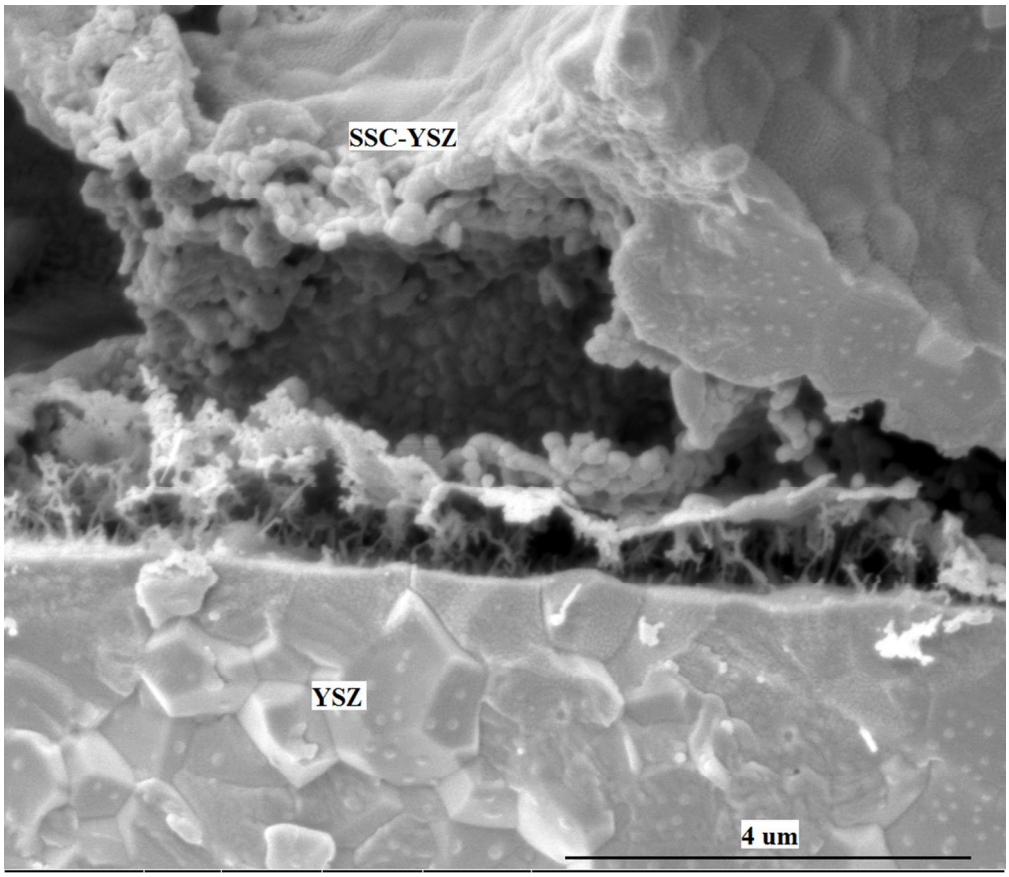

Fig. 8 (a) SEM micrograph of post-test cell under long-term steam electrolysis mode
302x261mm (86 x 86 DPI)

Faraday Discussions Accepted Manuscript

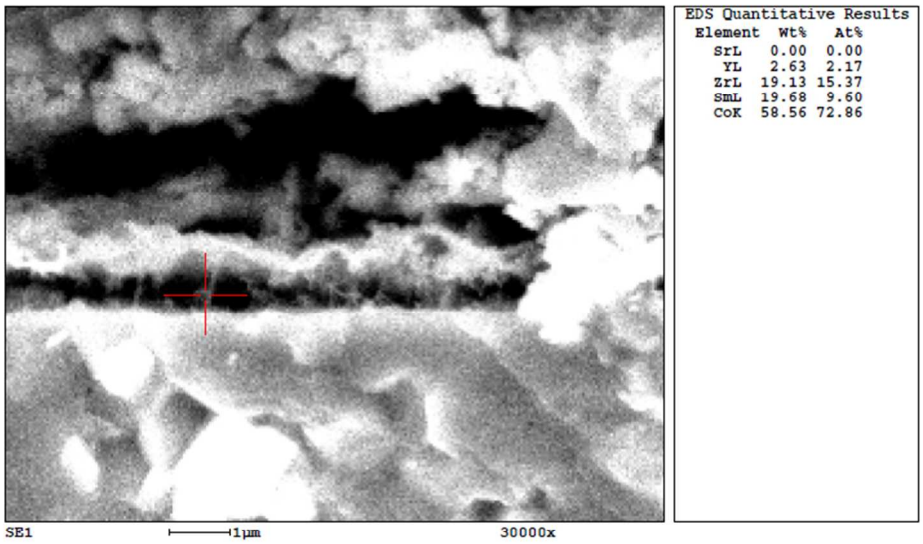

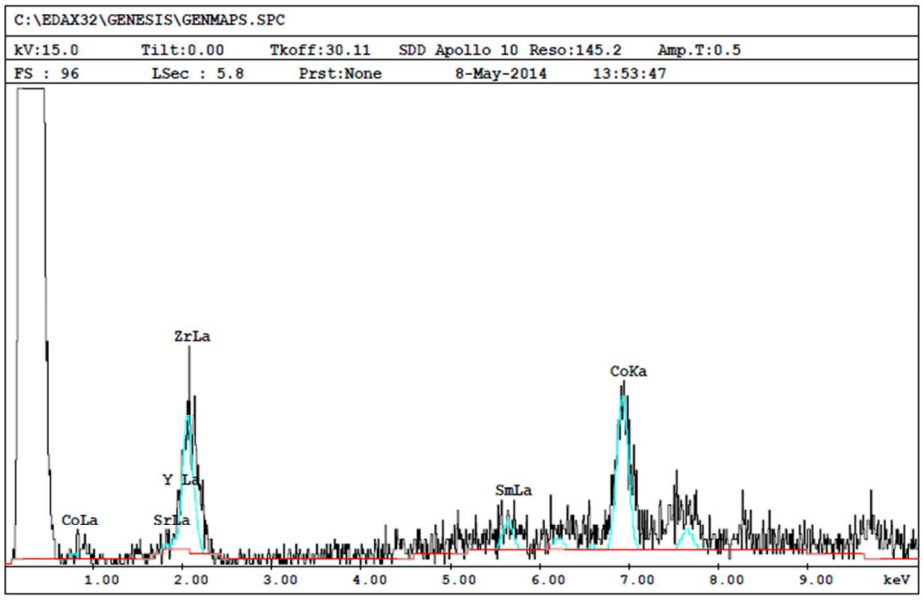

Figure 8(b) EDS spectrum of the selected area in the SEM image
199x246mm (96 x 96 DPI)

Faraday Discussions Accepted Manuscript